

# THE ROLE OF MULTIPLE CHARGE STATES IN ZINC DIFFUSION IN GALLIUM ARSENIDE

By

J.R. KING

Division of Theoretical Mechanics, School of Mathematical Sciences,  
University of Nottingham

and

M.G. MEERE\*

Department of Mathematical Physics, National University of Ireland, Galway

[Received 13 July 1998. Read 5 February 2001. Published 16 October 2001.]

## ABSTRACT

In this paper we provide a mathematical analysis of an effect whose significance for the diffusion of zinc in gallium arsenide has recently been indicated. The relevant model is of kick-out type and involves both doubly and triply charged self-interstitials; it can be written as a coupled pair of non-linear diffusion equations. Both numerical and asymptotic results are presented. It is found that the model is capable of reproducing much of the behaviour observed in experimental profiles. The singular perturbation analysis reveals the range of validity of the various regimes, as well as yielding other information about the diffusion processes.

## 1. Introduction

Modern semiconductor devices are given their electrical properties by introducing impurities into selected areas of the semiconductor substrate. The diffusion mechanisms which govern the redistribution of impurity in compound III–V semiconductors such as gallium arsenide (GaAs) are complex and involve the interaction of the impurity atoms with point defects, such as vacancies and self-interstitials, in the crystal. Self-interstitial atoms are host atoms which occupy interstitial sites in the crystal. Bosker *et al.* [2] have recently presented evidence for the significance of both doubly and triply negatively charged self-interstitials in determining the nature of the diffused profiles of zinc in gallium arsenide, zinc being one of the main impurities used to dope gallium arsenide. The purpose of this paper is to present an asymptotic analysis, using matched asymptotic expansions, which clarifies the various regimes involved, indicating their range of validity as well as quantifying the types of non-linear profile observed. Numerical solutions illustrating the asymptotic results are also given.

The model we study is a variant of the kick-out model originally proposed by Gosele and Morehead [3]; a more recent reference, which includes certain charge effects, is Yu *et al.* [11]. In the kick-out mechanism an interstitial atom becomes

---

\*Corresponding author, e-mail: martin.meere@nuigalway.ie

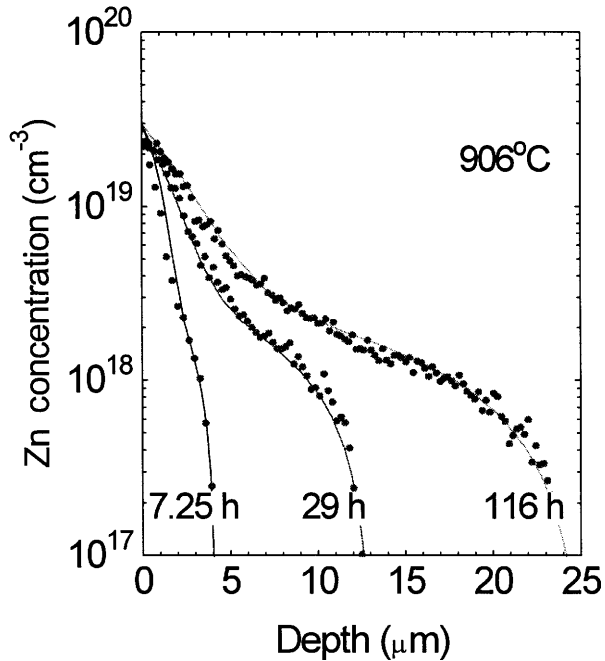


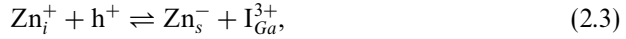
FIG. 1—Experimental Zn diffusion profiles in GaAs taken from Bosker *et al.* [2]. Diffusion times: 7.25h, 29h and 116h. The solid lines represent some of their numerical solutions of a kick-out model. Copyright (1995) by the American Physical Society.

substitutional by knocking a host atom into an interstitial site, the reverse process also being allowed. A substitutional impurity atom can move by first being knocked onto an interstitial site by a self-interstitial. The impurity atom can then diffuse interstitially before returning to the substitutional state by forcing a host atom into an interstitial site. In the present model, the self-interstitials come in two types, doubly and triply positively charged, and a derivation of the relevant governing equations is given below. These charge states have been suggested by experimental results [2] and are consistent with theoretical predictions [1]. More detailed descriptions of the kick-out mechanism can be found in [2], [3] and [11], which also contain other relevant references.

The diffusion of zinc in gallium arsenide is very complex, with a number of qualitatively different in-diffusion profiles being observed in experiments; see [11], in which three distinct categories of profiles for this system are identified. As indicated above, this complexity is due to the interaction between impurity and native defects in the crystal; the concentrations of the various defects are sensitive to the particular conditions of a given diffusion, leading to the wide variety of observed behaviours. A particularly interesting category of experimental profiles have a double concave shape; see Fig. 1, where we have reproduced experimental data of this kind from [2]. Bosker *et al.* [2] have shown that a kick-out model which incorporates both doubly and triply charged self-interstitials can reproduce the double concave behaviour, and this is confirmed by the mathematical analysis of this paper; see, in particular, Section 4 below.

## 2. Model and non-dimensionalisation

The species involved (see [2]) are zinc interstitials  $Zn_i^+$ , zinc substitutionals  $Zn_s^-$  and doubly and triply charged gallium self-interstitials  $I_{Ga}^{2+}$  and  $I_{Ga}^{3+}$ . We make the usual assumption that the relevant reactions



are in equilibrium,  $h^+$  denoting a hole. This leads (in view of the principle of detailed balance) to the two mass action relations

$$c_i = k_1 c_s c_2, \quad c_3 = k_2 c_2 p \quad (2.4)$$

where  $c_i = [Zn_i^+]$ ,  $c_s = [Zn_s^-]$ ,  $c_2 = [I_{Ga}^{2+}]$ ,  $c_3 = [I_{Ga}^{3+}]$ ,  $p = [h^+]$  and  $k_1$  and  $k_2$  are constants. Conservation of impurity implies that

$$\frac{\partial}{\partial t}(c_s + c_i) = D_i \frac{\partial}{\partial x} \left( \frac{\partial c_i}{\partial x} - \frac{c_i}{p} \frac{\partial p}{\partial x} \right), \quad (2.5)$$

where  $D_i$  is a constant (interstitial) diffusivity and the second term on the right-hand side is the usual drift term arising from the motion of charged particles in an electric field (see, for example, [11] and [5]). We thus also make the usual assumption that the diffusivity of the zinc substitutionals is negligible. Conservation of gallium similarly implies that

$$\frac{\partial}{\partial t}(c_2 + c_3 - c_s) = D_2 \frac{\partial}{\partial x} \left( \frac{\partial c_2}{\partial x} - \frac{2c_2}{p} \frac{\partial p}{\partial x} \right) + D_3 \frac{\partial}{\partial x} \left( \frac{\partial c_3}{\partial x} - \frac{3c_3}{p} \frac{\partial p}{\partial x} \right) \quad (2.6)$$

where the diffusivities  $D_2$  and  $D_3$  are also taken to be constant; the  $-c_s$  term appears on the left-hand side because when reactions (2.1) and (2.3) occur in the leftward direction the loss of a  $Zn_s^-$  coincides with the gain of a gallium atom on a lattice site. Equations (2.5)–(2.6) can alternatively be derived by initially not adopting the assumption of reaction equilibrium, writing down individual reaction-diffusion equations for each species, and taking appropriate combinations of these prior to letting the reaction rate coefficients tend to infinity (cf. [4]).

Finally, we assume charge neutrality

$$p + 2c_2 + 3c_3 + c_i = n + c_s, \quad (2.7)$$

where  $n = n_i^2/p$  is the electron concentration,  $n_i$  being a constant. This completes the model except for boundary and initial conditions; we treat the case of a surface source of impurity so that

$$\left. \begin{aligned} c_i &= c_i^*, c_2 = c_2^* (p/p^*)^2, c_3 = c_3^* (p/p^*)^3 \text{ on } x = 0, \\ c_i &\rightarrow 0, c_2 \rightarrow c_2^*, c_3 \rightarrow c_3^* \text{ as } x \rightarrow +\infty, \\ c_s &= c_i = 0, c_2 = c_2^*, c_3 = c_3^*, p = p^* \text{ at } t = 0 \end{aligned} \right\} \quad (2.8)$$

where  $x = 0$  is the semiconductor surface and the intrinsic concentrations  $c_2^*$  and  $c_3^*$  are related (see (2.4)) by

$$c_3^* = k_2 c_2^* p^*,$$

$p^*$  is the positive root of

$$p^* + 2c_2^* + 3c_3^* = n_i^*/p^*$$

(see (2.7)) and  $c_i^*$  is the concentration of interstitial impurity induced by the source. The conditions on  $x = 0$  in (2.8) imply that the surface is in equilibrium.

We non-dimensionalise by writing

$$\begin{aligned} c_s &= c_s^* \hat{c}_s, \quad c_i = c_i^* \hat{c}_i, \quad c_2 = c_2^* (P^*/p^*)^2 \hat{c}_2, \quad c_3 = c_3^* (P^*/p^*)^3 \hat{c}_3, \\ p &= P^* \hat{p}, \quad t = T \hat{t}, \quad x = \sqrt{D_i T c_i^*/c_s^*} \hat{x}, \end{aligned}$$

where  $P^* = (p)_{x=0}$  and  $c_s^* = c_i^*/k_1 c_2^* (P^*/p^*)^2$ ;  $P^*$  is given by

$$P^* + 2c_2^* (P^*/p^*)^2 + 3c_3^* (P^*/p^*)^3 + c_i = n_i^2/P^* + c_s^*. \quad (2.9)$$

Here  $T$  is some representative timescale. We note that, for the boundary and initial conditions (2.8), the solutions to (2.4), (2.5), (2.6) and (2.7) are self-similar, depending only on  $x/\sqrt{t}$ ; we prefer not to work in terms of the corresponding similarity ordinary differential equations since our asymptotic results are then almost immediately applicable to more general initial-boundary value problems. Henceforth we drop the hats, the dimensionless model then being:

$$\begin{aligned} c_i &= c_s c_2, \quad c_3 = c_2 p, \\ (1 + v^2 - \varepsilon_i - 2\varepsilon_2 - 3\varepsilon_3)p + \varepsilon_i c_i + 2\varepsilon_2 c_2 + 3\varepsilon_3 c_3 &= c_s + v^2/p, \\ \frac{\partial}{\partial t}(c_s + \varepsilon_i c_i) &= \frac{\partial}{\partial x} \left( \frac{\partial c_i}{\partial x} - \frac{c_i}{p} \frac{\partial p}{\partial x} \right), \\ \frac{\partial}{\partial t}(\varepsilon_2 c_2 + \varepsilon_3 c_3 - c_s) &= \gamma_2 \frac{\partial}{\partial x} \left( \frac{\partial c_2}{\partial x} - \frac{2c_2}{p} \frac{\partial p}{\partial x} \right) + \gamma_3 \frac{\partial}{\partial x} \left( \frac{\partial c_3}{\partial x} - \frac{3c_3}{p} \frac{\partial p}{\partial x} \right), \\ c_s = c_i = c_2 = c_3 = p &= 1 \text{ on } x = 0, \\ c_s, c_i \rightarrow 0, c_2 \rightarrow \delta^2, c_3 \rightarrow \delta^3, p \rightarrow \delta &\text{ as } x \rightarrow +\infty, \\ c_s = c_i = 0, c_2 = \delta^2, c_3 = \delta^3, p = \delta &\text{ at } t = 0, \end{aligned} \quad (2.10)$$

where

$$\begin{aligned} \varepsilon_i &= c_i^*/c_s^*, \quad \varepsilon_2 = c_2^* (P^*/p^*)^2 / c_s^*, \quad \varepsilon_3 = c_3^* (P^*/p^*)^3 / c_s^*, \\ \delta &= p^*/P^*, \quad v = n_i/\sqrt{P^* c_s^*}, \quad \gamma_2 = D_2 \varepsilon_2 / D_i \varepsilon_i, \quad \gamma_3 = D_3 \varepsilon_3 / D_i \varepsilon_i, \end{aligned}$$

where we have used (2.9). The values of these parameters are sensitive to the particular conditions of a given diffusion experiment and can vary considerably. However,  $\varepsilon_2$  and  $\varepsilon_3$  are usually small (as are  $\delta$  and  $\varepsilon_i$ ); for example, one of the experiments of [2] has  $\varepsilon_2, \varepsilon_3 = O(10^{-1})$  (and  $\gamma_2 = O(10^{-3})$ ,  $\gamma_3 = O(10^{-2})$ ). Moreover,

in their simulations they adopt parameter values corresponding to  $\gamma_2, \gamma_3$  lying in the ranges (a)  $\gamma_2 + \gamma_3 \gg 1$ , (b)  $\gamma_3 \ll \gamma_2 \ll 1$  and (c)  $\gamma_2 \ll \gamma_3 \ll 1$ , indicating the possible extent of variation of such quantities. Experimental data which illustrate the complexity of the Zn/GaAs system can be found in, for example, [10], [7], [9] and [2], the variety of qualitatively different profiles which arise again serving to emphasise the value of investigating in full the  $(\gamma_2, \gamma_3)$  parameter space. It will be seen that the model discussed here is capable of reproducing many of the features of the experimental profiles. The parameters are related by

$$(1 + v^2 - \varepsilon_i - 2\varepsilon_2 - 3\varepsilon_3)\delta + 2\varepsilon_2\delta^2 + 3\varepsilon_3\delta^3 = v^2/\delta. \quad (2.11)$$

In dimensionless terms, the supersaturations for the two species of self-interstitials are defined (cf. [2]) by

$$S_2 = c_2/p^2 \text{ and } S_3 = c_3/p^3. \quad (2.12)$$

Since we have assumed reaction equilibrium, we have  $S_2 = S_3$ .

### 3. Asymptotic analysis

#### 3.1. $\gamma_2 = \gamma_3 = O(1)$

*Introduction.* Two asymptotic limits need to be addressed to describe the required range of behaviour. The quantities  $\varepsilon_i, \varepsilon_2, \varepsilon_3, v$  and  $\delta$  are all small in practice with, from (2.11),  $v \sim \delta$ . In this subsection we consider the case where the other quantities,  $\gamma_1$  and  $\gamma_2$ , are  $O(1)$ . As indicated in [2], this will enable us to characterise the variety of diffused profiles which the model may predict. A numerical solution for the defect concentrations for this parameter regime is illustrated in Fig. 2; it may be helpful to refer to this in the subsequent analysis. The system was integrated numerically using a simple explicit time-stepping procedure on a uniform mesh, standard finite difference approximations being used for the derivatives. Time-stepping is applied to equations (2.10)<sub>3</sub> and (2.10)<sub>4</sub> and the remaining (algebraic) equations then used in determining the values of each of the dependent variables at the new time-step; sufficient grid points were used to capture any rapid variation in the behaviour. It should be noted that, for the high concentration regions, the substitutional concentration is essentially the total impurity concentration since  $\varepsilon_i$  is small. We now describe the asymptotic structure for this regime.

*High concentration (surface) region.* The most important region in practical terms is the surface region  $x = O(1)$ . Adding the third and fourth equations of (2.10) and taking  $\varepsilon_i, \varepsilon_2, \varepsilon_3, v, \delta \rightarrow 0$  gives to leading order

$$p = c_s, \quad c_2 = c_i/c_s, \quad c_3 = c_i \quad (3.1)$$

and, integrating once,

$$\frac{\partial c_i}{\partial x} - \frac{c_i}{p} \frac{\partial p}{\partial x} + \gamma_2 \left( \frac{\partial c_2}{\partial x} - \frac{2c_2}{p} \frac{\partial p}{\partial x} \right) + \gamma_3 \left( \frac{\partial c_3}{\partial x} - \frac{3c_3}{p} \frac{\partial p}{\partial x} \right) = 0; \quad (3.2)$$

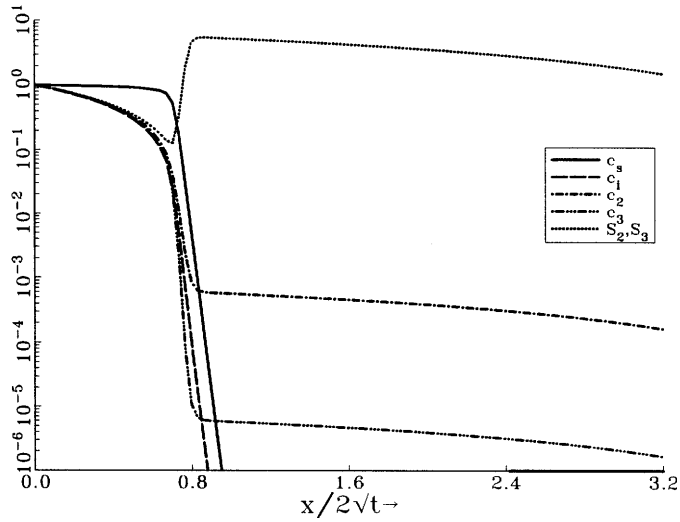


FIG. 2—A numerical solution corresponding to case (a) of [2]; the parameter values are  $\gamma_2 = \gamma_3 = 1.0$ ,  $\varepsilon_i = \varepsilon_2 = \varepsilon_3 = \nu = 0.01$ .

the right-hand side of (3.2) must be zero in order to match into the regions below. Hence

$$\left(1 + \frac{\gamma_2}{c_s} + \gamma_3\right) \frac{dc_i}{dc_s} = \left(\frac{1}{c_s} + \frac{3\gamma_2}{c_s^2} + \frac{3\gamma_3}{c_s}\right) c_i,$$

which is separable and, using  $c_s = c_i = 1$  on  $x = 0$ , yields

$$c_i = (1 + \gamma_2 + \gamma_3)^{\frac{2}{1+\gamma_3}} c_s^3 / (\gamma_2 + (1 + \gamma_3)c_s)^{\frac{2}{1+\gamma_3}} \tag{3.3}$$

and hence

$$\frac{\partial c_s}{\partial t} = \frac{\partial}{\partial x} \left( D_{eff}(c_s) \frac{\partial c_s}{\partial x} \right) \tag{3.4}$$

where the effective diffusivity is given by

$$D_{eff}(c_s) = 2(1 + \gamma_2 + \gamma_3)^{\frac{2}{1+\gamma_3}} c_s^2 (\gamma_2 + \gamma_3 c_s) / (\gamma_2 + (1 + \gamma_3)c_s)^{\frac{3+\gamma_3}{1+\gamma_3}}. \tag{3.5}$$

Equation (3.4) is to be solved subject to

$$\begin{aligned} c_s &= 1 \text{ on } x = 0, \\ c_s &\rightarrow 0 \text{ as } x \rightarrow +\infty, \\ c_s &= 0 \text{ at } t = 0. \end{aligned}$$

The expression (3.5) is the main result of this subsection, containing cases (a)–(c) of [2] as limit cases and embodying the full range of diffused profiles illustrated there.

Limit cases of (3.5) are

$$(i) \gamma_2 \gg 1 \text{ or } \gamma_3 \gg 1 \quad D_{eff} \sim 2c_s^2; \quad (3.6)$$

$$(ii) \gamma_2 \ll 1 \text{ and } \gamma_3 \ll 1 \quad D_{eff} \sim 2(\gamma_3 c_s + \gamma_2)/c_s. \quad (3.7)$$

Here (i) is equivalent to case (a), and (ii) incorporates cases (b) and (c), of [2]. The second limit is a particularly significant one, as we shall see below. The expression (3.7) holds for  $c_s = O(1)$  but is not uniformly valid: for all  $\gamma_2, \gamma_3$  we have from (3.5) that

$$D_{eff} \sim 2 \left( (1 + \gamma_2 + \gamma_3)/\gamma_2 \right)^{\frac{2}{1+\gamma_3}} c_s^2 \text{ as } c_s \rightarrow 0 \quad (3.8)$$

which is degenerate, so that the solution to (3.4) is compactly supported with  $c_s \equiv 0$  for  $x \geq q(t)$ , say. In case (ii), (3.7) must thus be supplemented with

$$D_{eff} \sim 2\gamma_2 c_s^2 / (c_s + \gamma_2)^3 \text{ for } c_s = O(\gamma_2),$$

and a uniformly valid representation for  $\gamma_2, \gamma_3 \ll 1$  is thus

$$D_{eff} \sim 2c_s^2(\gamma_3 c_s + \gamma_2) / (c_s + \gamma_2)^3. \quad (3.9)$$

This is a non-monotonic function of  $c_s$ , providing an explanation of the kinked types of profile observed in practice (cf. Fig. 3; the diffused profiles there should be contrasted with those of Fig. 2).

Effective diffusivities can be obtained from experimental profiles by using Boltzmann–Matano analysis; see, for example, [8]. Fitting (3.5) to a diffusivity obtained in that fashion would make possible the estimation of the physical parameters.

*Transition layer.* When  $c_s$  becomes of  $O(v)$  the balance in the charge neutrality condition becomes more complex. This happens for  $z = O(1)$ , where  $x = q(t) + v^2 z$  and  $q(t)$  is given asymptotically by the edge of the support of the solution to (3.4). The other scalings required are

$$c_s = vC_s, c_i = v^3 C_i, c_2 = v^2 C_2, c_3 = v^3 C_3, p = vP$$

and, to leading order,

$$\begin{aligned} C_i &= C_s C_2, \quad C_3 = C_2 P, \quad P = C_s + 1/P, \\ \frac{\partial}{\partial z} \left( \frac{\partial C_i}{\partial z} - \frac{C_i}{P} \frac{\partial P}{\partial z} \right) &= -\dot{q} \frac{\partial C_s}{\partial z}, \\ \frac{\partial}{\partial z} \left( \frac{\partial C_2}{\partial z} - \frac{2C_2}{P} \frac{\partial P}{\partial z} \right) &= 0. \end{aligned} \quad (3.10)$$

Matching with the surface region yields

$$C_2 = \left( (1 + \gamma_2 + \gamma_3)/\gamma_2 \right)^{\frac{2}{1+\gamma_3}} P^2, \quad (3.11)$$

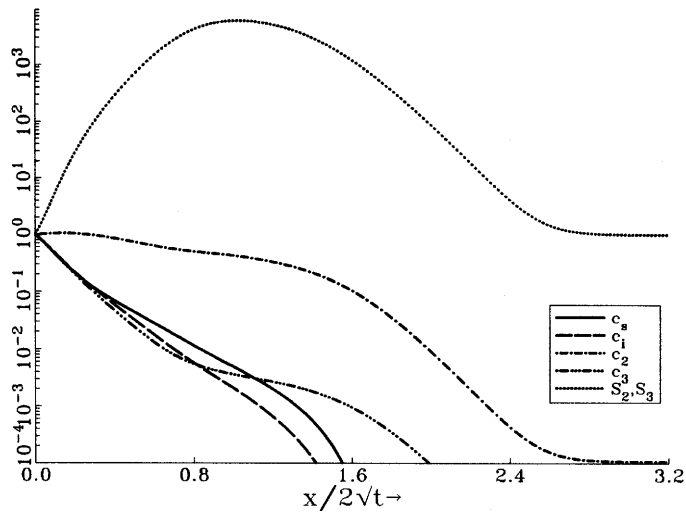


FIG. 3—A numerical solution corresponding to case (b) of [2]; the parameter values are  $\gamma_2 = \gamma_3 = 0.005$ ,  $\varepsilon_i = \varepsilon_2 = \varepsilon_3 = \nu = 0.01$ .

implying from (3.10) an effective diffusivity for  $C_s$  of

$$D_{eff}(C_s) = ((1 + \gamma_2 + \gamma_3)/\gamma_2)^{\frac{2}{1+\gamma_3}} \left( C_s + \sqrt{C_s^2 + 4} \right)^3 / 4\sqrt{C_s^2 + 4}, \tag{3.12}$$

which matches with (3.5) for large  $C_s$  but is bounded away from zero. Equation (3.10) can be integrated to yield

$$((1 + \gamma_2 + \gamma_3)/\gamma_2)^{\frac{2}{1+\gamma_3}} (P^2 + \ln(P^2 - 1)) = -qz.$$

*Outer region.* Here we have  $x = \varepsilon_2^{-\frac{1}{2}} X$ ,  $c_s$  and  $c_i$  are exponentially small and the self-interstitial concentrations drop back to their equilibrium values, as required by (2.10). Scaling according to

$$c_2 = \delta^2 c_2^\dagger, c_3 = \delta^3 c_3^\dagger, p = \delta^2 p^\dagger$$

gives at leading order

$$\begin{aligned} c_3^\dagger &= c_2^\dagger, p^\dagger = 1, \\ \frac{\partial c_2^\dagger}{\partial t} &= \gamma_2 \frac{\partial^2 c_2^\dagger}{\partial X^2}, \\ c_2^\dagger &= ((1 + \gamma_2 + \gamma_3)/\gamma_2)^{\frac{2}{1+\gamma_3}} \text{ on } X = 0, \\ c_2^\dagger &\rightarrow 1 \text{ as } X \rightarrow +\infty, \\ c_2^\dagger &= 1 \text{ at } t = 0 \end{aligned} \tag{3.13}$$

where we have used from (2.11) that  $v \sim \delta$  and have matched using (3.11). Hence

$$c_2^\dagger = \left( (1 + \gamma_2 + \gamma_3) / \gamma_2 \right)^{\frac{2}{1+\gamma_3}} \operatorname{erfc} \left( X / \sqrt{2\gamma_2 t} \right) + \operatorname{erf} \left( X / \sqrt{2\gamma_2 t} \right).$$

The condition on  $X = 0$  quantifies the degree of self-interstitial supersaturation.

3.2.  $\gamma_2 = O(\varepsilon_2), \gamma_3 = O(\varepsilon_3)$

*Introduction.* The limit discussed here is of particular physical significance, enabling us to analyse physical effects, such as electrical compensation of  $Zn_s^-$  by  $I_{Ga}^{2+}$ , indicated in [2]. We note that there are serious difficulties in treating such effects numerically, both because the system is highly stiff and because it is necessary in practice to calculate the impurity profile over many orders of magnitude, but that they are amenable to the asymptotic approach we now outline. We write  $\gamma_2 = \Gamma_2 \varepsilon_2, \gamma_3 = \Gamma_3 \varepsilon_3$ , this choice of scalings being based on the assumption that  $D_2$  and  $D_3$  are comparable. We assume that  $\varepsilon_2 / \varepsilon_3 = O(1)$ .

In Fig. 3 we plot a numerical solution for the substitutional concentration for this parameter regime, this case corresponding to case (b) of [2].

*High concentration region.* Writing  $x = (\Gamma_2 \varepsilon_2)^{\frac{1}{2}} y$ , the leading order problem is

$$\begin{aligned} c_i = p = c_s = c_3, \quad c_2 = 1, \\ \frac{\partial c_s}{\partial t} = \frac{\partial}{\partial y} \left( 2 \left( \frac{1}{c_s} + \frac{\Gamma_3 \varepsilon_3}{\Gamma_2 \varepsilon_2} \right) \frac{\partial c_s}{\partial y} \right). \end{aligned} \tag{3.14}$$

In order to match, the non-linear diffusion equation (3.14) is to be solved subject to

$$\begin{aligned} c_s = 1 \quad \text{on } y = 0, \\ c_s \rightarrow 0, \quad c_s^{-1} \frac{\partial c_s}{\partial y} \rightarrow 0 \quad \text{as } y \rightarrow +\infty, \\ c_s = 0 \quad \text{at } t = 0; \end{aligned}$$

it contains the expected form of effective diffusivity (cf. (3.7)). We have

$$c_s \sim 4t / y^2 \quad \text{as } y \rightarrow +\infty.$$

*Outer region.* We scale

$$x = \Gamma_2^{\frac{1}{2}} Y, \quad c_s = \varepsilon_2 C_s, \quad c_i = \varepsilon_2 C_i, \quad p = \varepsilon_2 P, \quad c_2 = C_2, \quad c_3 = \varepsilon_2 C_3$$

to give to leading order, if  $\delta \ll \varepsilon_2$ ,

$$C_i = C_s C_2, \quad C_3 = C_2 P, \tag{3.15}$$

$$P + 2C_2 = C_s, \tag{3.16}$$

$$\Gamma_2 \frac{\partial C_s}{\partial t} = \frac{\partial}{\partial Y} \left( \frac{\partial C_i}{\partial Y} - \frac{C_i}{P} \frac{\partial P}{\partial Y} \right), \tag{3.17}$$

$$\frac{\partial}{\partial t} (C_2 - C_s) = \frac{\partial}{\partial Y} \left( \frac{\partial C_2}{\partial Y} - \frac{2C_2}{P} \frac{\partial P}{\partial Y} \right); \tag{3.18}$$

electrical compensation (i.e. the significant reduction in hole concentration below the substitutional impurity concentration) at diffusion temperatures due to doubly charged self-interstitials is clear from (3.16). Further analytical progress is not possible as it stands, but we now exploit the further limit  $\Gamma_2 \rightarrow 0$ , which is also justifiable on physical grounds ([2]). We then have from (3.17) that, to leading order,  $C_i = P$ , so

$$C_2 = C_s/(C_s + 2), \quad C_i = P = C_s^2/(C_s + 2), \quad C_3 = C_s^3/(C_s + 2)^2,$$

and (3.18) leads to the single non-linear diffusion equation

$$\begin{aligned} \frac{\partial}{\partial t} \left( \frac{C_s(C_s + 1)}{(C_s + 2)} \right) &= \frac{\partial}{\partial Y} \left( \frac{2(C_s + 3)}{(C_s + 2)^2} \frac{\partial C_s}{\partial Y} \right), \\ C_s &\sim 4t/Y^2 \text{ as } Y \rightarrow 0^+, \\ C_s &\rightarrow 0 \text{ as } Y \rightarrow +\infty, \\ C_s &= 0 \text{ at } t = 0, \end{aligned} \tag{3.19}$$

from which an effective diffusivity, which may again be assessed against experimental profiles and is bounded away from zero, can be obtained. We note that  $C_2 \sim C_s/2$  holds as  $Y \rightarrow +\infty$ , so that almost exact electrical compensation occurs in the far-field.

The structure of the solution to (3.15)–(3.18) in the limit  $\Gamma_2 \rightarrow 0$  contains two further (narrow) regions at large  $Y$ ; the need for such interior layers is made clear by noting that the solution to (3.15)–(3.18) is in fact compactly supported, with  $C_i = C_2 = C_s = P = 0$  for  $Y \geq Q(t)$  for some  $Q(t)$  (and  $C_s = O(P)$ ,  $C_2 = O(P^2)$ ,  $C_i = O(P^3)$  as  $Y \rightarrow Q^-$ ). Close to  $Q(t)$  the solution to (2.10) contains other narrow regions in which  $c_2$  and  $c_3$  drop to the values required by (2.10). All of these layers are of very low impurity concentration and we omit details. We should note here that the solution to the full problem (2.10) is not in fact compactly supported, but does have very abrupt impurity fronts for the physically relevant parameter regimes (see Section 4).

In view of formulations such as (3.19), some comments concerning Boltzmann–Matano analysis are in order. Quantities which can be measured experimentally include the total impurity profile (here  $C_s$  to leading order) and the carrier concentration. These often satisfy equations of the form (cf. (3.19))

$$-\frac{1}{2}\eta \frac{d}{d\eta} (F(u)) = \frac{d}{d\eta} \left( D(u) \frac{du}{d\eta} \right) \tag{3.20}$$

where  $\eta = x/t^{1/2}$ . It follows from (3.20) that

$$D(u) = -\frac{1}{2} \frac{d\eta}{du}(u) \int_0^u \eta(u') \frac{dF}{du}(u') du'. \tag{3.21}$$

In the conventional cases in which the Boltzmann–Matano technique is applied we have  $F(u) = u$  and (3.21) enables  $D(u)$  to be determined by measuring  $\eta(u)$ ; more generally, however, (3.21) merely provides one relationship between  $D$  and  $F$  and

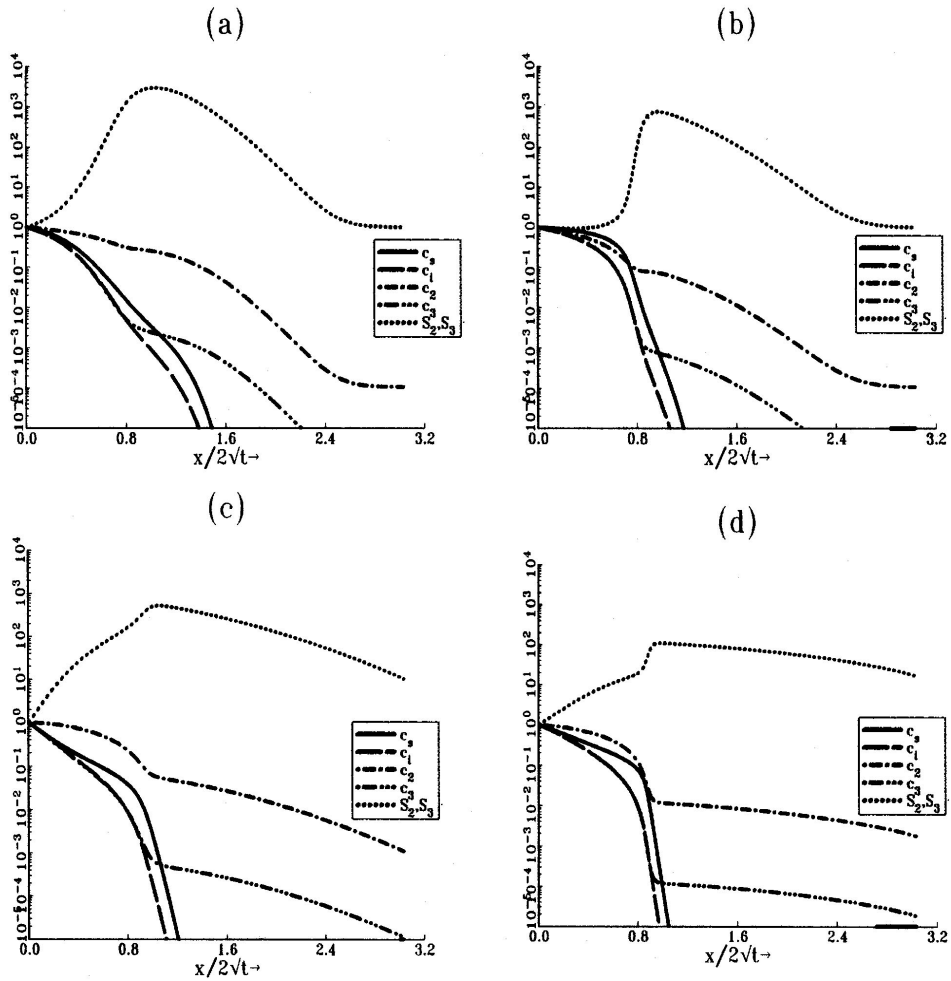


FIG. 4—Numerical solutions of (10) for parameter values  $\epsilon_i = \epsilon_2 = \epsilon_3 = \nu = 0.01$  and  
 (a)  $\gamma_2 = 0.005, \gamma_3 = 0.05$ , (b)  $\gamma_2 = 0.005, \gamma_3 = 0.2$ , (c)  $\gamma_2 = 0.02, \gamma_3 = 0.005$  and  
 (d)  $\gamma_2 = 0.05, \gamma_3 = 0.005$ .

specific assumptions concerning the diffusion mechanism, such as those which have led us to (3.19), must be adopted in order for  $F$  and  $D$  to be determined separately.

#### 4. Discussion

In this paper we have analysed a version of the kick-out model involving both doubly and triply charged self-interstitials, a system which has been previously proposed for the technologically important Zn/GaAs system. We begin the discussion by referring to some further numerical results (Figs 4 and 5) since these will feature again below. Inspecting Figs 2 and 3, it is clear that there can be a dramatic difference in the diffusion behaviour between those cases for which  $\gamma_2, \gamma_3 = O(1)$  and those for which  $\gamma_2, \gamma_3 \ll 1$ . In view of this, it is clearly of interest to investigate the

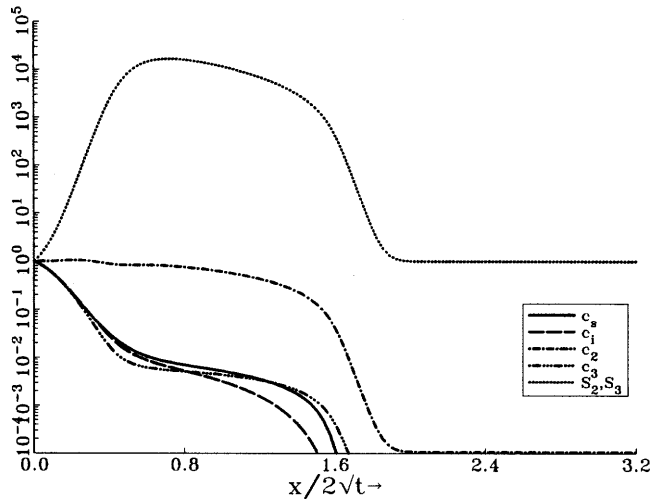


FIG. 5—Numerical solution of equations (10) illustrating doubly concave shape of impurity profiles. The parameter values are  $\gamma_2 = 0.001$ ,  $\gamma_3 = 0.01$ ,  $\varepsilon_i = \varepsilon_2 = \varepsilon_3 = \nu = 0.01$ .

behaviour for some intermediate regimes for  $\gamma_2$  and  $\gamma_3$ . In Fig. 4 we plot numerical solutions for four such cases, Fig. 4(c) capturing best the transition between the behaviours illustrated in Figs 2 and 3. Some of the features of the impurity curves illustrated in Fig. 4 can be explained using the appropriate effective diffusivity for the substitutionals and some discussion of this is given below. We note the distinctive character of the self-interstitial and self-interstitial supersaturation curves in each of the four graphs.

In Fig. 5 we plot a numerical solution of particular interest, for which  $\gamma_2 \ll \gamma_3 \ll 1$ . The impurity profiles have a doubly concave shape, of a type which has often been observed in experimental profiles; see, for instance, [9], [7] and [6]. In [6] the doubly concave shape was explained using a model which involved two charge states for the impurity interstitials rather than the self-interstitials, which they took to be singly positively charged; our results indicate that the current model provides a plausible alternative mechanism. The nature of the impurity profile displayed in Fig. 5 can be explained using the effective diffusivity for the substitutionals (see below).

One of the principal results of this paper is the derivation of an effective diffusivity which encompasses (a)–(c) of [2]. In the high concentration surface region, in which  $c_s/c_s^* = O(1)$ , this diffusivity (3.5) takes the dimensional form

$$D_{eff}(c_s) = \frac{2(1 + \gamma_2 + \gamma_3)^{\frac{2}{1+\gamma_3}} (\gamma_2 + \gamma_3 c_s/c_s^*)}{(\gamma_2 + (1 + \gamma_3)c_s/c_s^*)^{\frac{3+\gamma_3}{1+\gamma_3}}} \frac{c_s^2}{c_s^{*2}} \frac{c_i^*}{c_s^*} D_i, \tag{4.1}$$

while in the low concentration tail region, with  $c_s/c_s^* = O(\nu) \ll 1$ , we have from

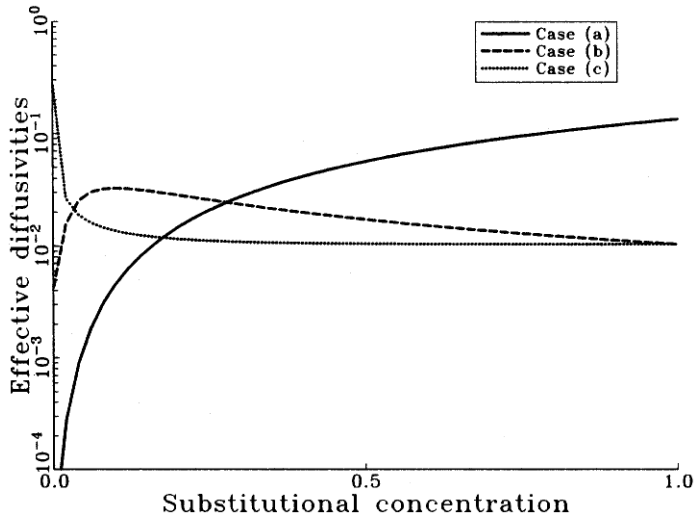


FIG. 6—Plots of the effective diffusivity for the substitutionals as given by (36). We plot  $c_s/c_s^*$  against  $D_{eff}(c_s/c_s^*)/D_i$  for  $v = 0.01$ ,  $c_i^*/c_s^* = 0.1$  and with (a)  $\gamma_2 = \gamma_3 = 1$ , (b)  $\gamma_2 = 0.1$ ,  $\gamma_3 = 0.01$ , (c)  $\gamma_2 = 0.01$ ,  $\gamma_3 = 0.1$ .

(3.12) the dimensional form

$$D_{eff}(c_s) = \frac{((1 + \gamma_2 + \gamma_3)/\gamma_2)^{\frac{2}{1+\gamma_3}} \left(c_s/c_s^* + \sqrt{c_s^2/c_s^{*2} + 4v^2}\right)^3}{4\sqrt{c_s^2/c_s^{*2} + 4v^2}} \frac{c_i^*}{c_s^*} D_i. \quad (4.2)$$

It is useful to give a single composite expression which we construct from (4.1)–(4.2) as a multiplicative composite, in the form

$$D_{eff}(c_s) = \frac{(1 + \gamma_2 + \gamma_3)^{\frac{2}{1+\gamma_3}} (\gamma_2 + \gamma_3 c_s/c_s^*) \left(c_s/c_s^* + \sqrt{c_s^2/c_s^{*2} + 4v^2}\right)^3}{4 (\gamma_2 + (1 + \gamma_3)c_s/c_s^*)^{\frac{3+\gamma_3}{1+\gamma_3}} \sqrt{c_s^2/c_s^{*2} + 4v^2}} \frac{c_i^*}{c_s^*} D_i. \quad (4.3)$$

We note that this effective diffusivity is bounded away from zero, with

$$D_{eff}(c_s = 0) = ((1 + \gamma_2 + \gamma_3)/\gamma_2)^{\frac{2}{1+\gamma_3}} v^2 \frac{c_i^*}{c_s^*} D_i, \quad (4.4)$$

and solutions for the diffusivity (4.2) are therefore not compactly supported. However, (4.4) is in practice often extremely small compared to  $D_i$  since  $v$  and  $c_i^*/c_s^*$  are usually small, leading to solutions with rather abrupt fronts, as described above. In Fig. 6 we plot the effective diffusivity (4.3) for three sets of values of  $\gamma_2$  and  $\gamma_3$  which relate to cases (a), (b), (c) of [2]; it is noteworthy that for each of these cases the diffusivity has a very different character, accounting for the distinctive nature of the impurity profiles for each of the three regimes.

We now note some important limiting cases of the above composite expression.

When either  $\gamma_2 \gg 1$  or  $\gamma_3 \gg 1$  we have

$$D_{eff}(c_s) \sim \frac{\left(c_s/c_s^* + \sqrt{c_s^2/c_s^{*2} + 4v^2}\right)^3}{4\sqrt{c_s^2/c_s^{*2} + 4v^2}} \frac{c_i^*}{c_s^*} D_i. \quad (4.5)$$

It is noteworthy that this effective diffusivity does not depend on  $D_2$  or  $D_3$ , the diffusivities for the self-interstitials. From Section 2 we recall that  $\gamma_2 = D_2\varepsilon_2/D_i\varepsilon_i$  and  $\gamma_3 = D_3\varepsilon_3/D_i\varepsilon_i$ , so the current limit may be interpreted as that in which the rate limiting step in the incorporation of substitutional impurity into the crystal is the relatively slow in-diffusion of the interstitial impurity from the surface. From (4.5), we have in the high concentration region  $c_s/c_s^* = O(1)$  that

$$D_{eff} \sim 2 \left(\frac{c_s}{c_s^*}\right)^2 \frac{c_i^*}{c_s^*} D_i$$

and this power law expression explains the ‘box-type’ shape for the impurity profiles which are obtained numerically in this regime (Fig. 6, case (a)).

Another limit of interest which gives rise to impurity profiles with a distinct character is  $\gamma_2 \ll 1$  and  $\gamma_3 \ll 1$ , which may be interpreted as rapid in-diffusion of impurity from the surface. In this limit, the effective diffusivity is given in dimensional terms by

$$D_{eff}(c_s) \sim \frac{\left(c_s/c_s^* + \sqrt{c_s^2/c_s^{*2} + 4v^2}\right)^3}{4\sqrt{c_s^2/c_s^{*2} + 4v^2}} \frac{(D_2\varepsilon_2 + D_3\varepsilon_3c_s/c_s^*)}{\varepsilon_i} \left(\frac{c_s^*}{c_s}\right)^3 \frac{c_i^*}{c_s^*}, \quad (4.6)$$

which does not depend on the impurity interstitial diffusivity  $D_i$ . In the high concentration region  $c_s/c_s^* = O(1)$  we have

$$D_{eff}(c_s) \sim \frac{2(D_2\varepsilon_2c_s^*/c_s + D_3\varepsilon_3)}{\varepsilon_i} \frac{c_i^*}{c_s^*}. \quad (4.7)$$

Two distinct subcases are worthy of mention here. Firstly, if  $1 \gg \gamma_2 \gg \gamma_3$  then (4.7) gives

$$D_{eff} \sim 2D_2 \frac{\varepsilon_2}{\varepsilon_i} \frac{c_i^*}{c_s},$$

and this fast diffusion (negative power law) form accounts for the convex shape in the calculated shape for the impurity profile in the surface region for this parameter regime. This is illustrated in the numerical solution displayed in Fig. 4 (c), where the convex shape of the substitutional profile near  $x = 0$  is clear. In Fig. 6, case (b), an effective diffusivity is plotted for this regime which exhibits the  $1/c_s$  behaviour for higher concentrations. For lower concentrations, the effective diffusivity drops to the value given by (4.4).

The second subcase of (4.7) which we discuss is  $1 \gg \gamma_3 \gg \gamma_2$  and we then have constant diffusivity

$$D_{eff}(c_s) \sim 2D_3 \frac{\varepsilon_3}{\varepsilon_i} \frac{c_i^*}{c_s^*},$$

leading to the classical complementary error function shape in the diffused profiles. The effective diffusivity for this regime is plotted in Fig. 6, case (c), where the expected behaviour is reproduced. Interestingly, the diffusivity is seen to rise steeply as  $c_s$  approaches zero and this is explained by inspecting equations (4.3) and (4.4) and noting the small value for  $\gamma_2$  chosen to obtain this plot. Numerical solutions for this regime are given in Fig. 4 (a) and Fig. 5, where the error function character of the substitutional profile near the surface is apparent.

We are now in a position to give an explanation of the impurity profiles displayed in Fig. 5 with  $1 \gg \gamma_3 \gg \gamma_2$  (see also the experimental data displayed in Fig. 1); it should be stressed that the significance of this parameter regime was identified by the asymptotic analysis. As already remarked, the diffusivity is approximately constant in the high concentration surface region  $c_s/c_s^* \gg D_2\varepsilon_2/D_3\varepsilon_3$  ( $= \gamma_2/\gamma_3 \ll 1$ ), explaining the erfc shape there. However, inspecting (4.7), we see that for  $c_s/c_s^* = O(D_2\varepsilon_2/D_3\varepsilon_3)$  the effective diffusivity is also contributed to by a  $c_s^*/c_s$  term. If we also recall the discussion of Section 3.1.2, we have that for  $(\gamma_2 =) D_2\varepsilon_2/D_i\varepsilon_i \ll c_s/c_s^* \ll D_2\varepsilon_2/D_3\varepsilon_3$  the effective diffusivity is dominated by the  $c_s^*/c_s$  term and hence the 'kink' in the intermediate part of the curves. Equation (3.9) gives the more complex dependence for the diffusivity when  $c_s/c_s^* = O(D_2\varepsilon_2/D_i\varepsilon_i)$ . However, for  $v \ll c_s/c_s^* \ll D_2\varepsilon_2/D_i\varepsilon_i$ , the diffusivity is approximately proportional to  $c_s^2$  and this accounts for the second concave region. For concentrations with  $c_s/c_s^* = O(v)$ , we recover an effective diffusivity of the form (4.2).

It should be noted that the governing system of equations which we study (see (2.10)) differs in a number of important respects from those implicit in [2]. In particular, we have assumed throughout that the kick-out reactions are in equilibrium and this led to a governing system of two non-linear diffusion equations and three algebraic relations. This system was integrated and we did not obtain the discrepancy between  $S_2$  and  $S_3$  in the far-field found in [2] in which reaction equilibrium was not enforced, leading to the numerical difficulties noted there.

In Fig. 2 we have plotted a numerical solution for  $\gamma_2 = \gamma_3 = 1$ . It is noteworthy that, for the regime  $\gamma_2 = \gamma_3 = O(1)$ , in the outer region where the impurity concentrations are exponentially small, the self-interstitial supersaturations are monotonically decreasing (see (3.13)). The maximum value of  $c_2$  is given at leading order by

$$\left( (D_i\varepsilon_i + D_2\varepsilon_2 + D_3\varepsilon_3) / D_2\varepsilon_2 \right)^{\frac{2D_i\varepsilon_i}{D_i\varepsilon_i + D_3\varepsilon_3}},$$

which is a convenient way of quantifying the degree of self-interstitial supersaturation.

In Section 3.2 we considered the case  $\gamma_2 = O(\varepsilon_2)$ ,  $\gamma_3 = O(\varepsilon_3)$ , in which a more complicated balance occurs in the outer region. As noted above, the regime  $\gamma_2, \gamma_3 \ll 1$  corresponds to the relatively rapid in-diffusion of impurity interstitials from the surface and is of physical relevance; considering this limit enabled us to quantify another effect noted in [2], namely the electrical compensation of negatively charged substitutionals by doubly charged self-interstitials over part of the diffused profile. The expression for charge neutrality, (2.7), implies that  $p \approx c_s$  in the high concentration regions. Interestingly, however, for the scaling considered in Section 3.2 the analysis reveals that, some way into the semiconductor, the substitutionals

are balanced by self-interstitials as well as holes, with  $p + 2c_2 \approx c_s$ . Even further in, the substitutionals can be balanced almost entirely by the doubly charged self-interstitials, so that  $2c_2 \approx c_s$ , implying almost complete electrical compensation in that region.

We conclude by noting that our analysis may also allow the convenient estimation of physical parameters appearing in the model. The identification of a uniformly valid effective diffusivity combined with the use of Boltzmann–Matano analysis on experimental impurity profiles would allow the estimation of model parameters.

#### ACKNOWLEDGEMENTS

The authors are grateful to the British Council/Enterprise Ireland for the award of a grant; MGM is also grateful to the Royal Society and the Royal Irish Academy for a travel grant. We thank N.A. Stolwijk for providing Fig. 1.

#### REFERENCES

- [1] G.A. Baraff and M. Schluter, Electronic structure, total energies, and abundances of the elementary point defects in GaAs, *Physical Review Letters* **55** (1985), 1327–30.
- [2] G. Bosker, N.A. Stolwijk, H.G. Hettwer, A. Rucki, W. Jager and U. Sodervall, Use of zinc diffusion into GaAs for determining properties of gallium interstitials, *Physical Review B* **52** (1995), 11927–31.
- [3] U. Gosele and F. Morehead, Diffusion of zinc in gallium arsenide: a new model, *Journal of Applied Physics* **52** (1981), 4617–19.
- [4] J.R. King and M.G. Meere, Asymptotic analysis of a combined dissociative and kick-out diffusion mechanism, *IMA Journal of Applied Mathematics* **56** (1996), 33–63.
- [5] J.R. King and M.G. Meere, The dissociative diffusion mechanism with charge effects I: One-dimensional in-diffusion, *The Quarterly Journal of Mechanics and Applied Mathematics* **54** (2001), 469–500.
- [6] S. Reynolds, D.W. Vook and J.F. Gibbons, Open-tube Zn diffusion in GaAs using diethylzinc and trimethylarsenic: experiment and model, *Journal of Applied Physics* **63** (1988), 1052–9.
- [7] C.H. Ting and G.L. Pearson, Time-dependence of zinc diffusion in gallium arsenide under a concentration gradient, *Journal of the Electrochemical Society: Solid State Science* **118** (1971), 1454–8.
- [8] B. Tuck, *Atomic diffusion in III–V semiconductors*, Adam Hilger, Bristol and Philadelphia, 1988.
- [9] B. Tuck and M.A. Kadhim, Anomalous diffusion profiles of zinc in GaAs, *Journal of Materials Science* **7** (1972), 585–91.
- [10] H.R. Winteler, Die diffusion von Zink und Gallium in Galliumarsenid bei 1100°C, *Helvetica Physica Acta* **44** (1971), 451–86.
- [11] S. Yu, T.Y. Tan and U. Gosele, Diffusion mechanism of zinc and beryllium in gallium arsenide, *Journal of Applied Physics* **69** (1991), 3547–65.